ACS Photonics

Article

pubs.acs.org/journal/apchd5

Scattering Dark States in Multiresonant Concentric Plasmonic Nanorings

Rasoul Alaee,*[,†,‡,#] Dennis Lehr,[§,#] Robert Filter,[‡] Falk Lederer,[‡] Ernst-Bernhard Kley,[§] Carsten Rockstuhl,[†,∥] and Andreas Tünnermann[§,⊥]

[†]Institute of Theoretical Solid State Physics, Karlsruhe Institute of Technology, Wolfgang-Gaede-Str. 1, 76128 Karlsruhe, Germany

[‡]Institute of Condensed Matter Theory and Solid State Optics, Abbe Center of Photonics, Friedrich-Schiller-University Jena, Max-Wien-Platz 1, 07743 Jena, Germany

[§]Institute of Applied Physics, Abbe Center of Photonics, Friedrich-Schiller-University Jena, Max-Wien-Platz 1, 07743 Jena, Germany

[∥]Institute of Nanotechnology, Karlsruhe Institute of Technology, P.O. Box 3640, 76021 Karlsruhe, Germany

[⊥]Fraunhofer Institute for Applied Optics and Precision Engineering IOF, Albert-Einstein-Str. 7, 07745 Jena, Germany

ABSTRACT: Plasmonic nanoantennas can feature a sophisticated spectral response that may be the springboard for a plethora of applications. Particularly, spectrally sharp Fano resonances have been at the focus of interest because of their promising applications in sensing. Usually, the observation of Fano resonances requires nanostructures that exhibit multiple plasmonic resonances such as higher-order multipole moments. We show that similar spectral features can be observed with nanoantennas sustaining solely electric-dipolar resonances. The considered nanoantennas consist of multiple concentric gold nanorings separated by thin dielectric spacers. These nanoantennas host multiple resonances with disparate line widths in the visible and near-infrared. We theoretically and experimentally show that the interference of these resonances causes Fano features and scattering dark states. The electric-dipolar character permits the use of a simplified dense-array theory to predict the response of arrays of such nanoantennas from the electric polarizability of the individual constituents. This paves the way for a simplified design of plasmonic metasurfaces.

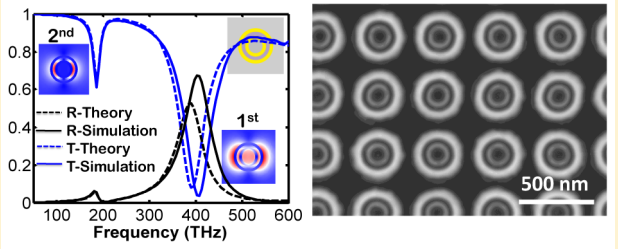

KEYWORDS: *scattering dark states, plasmonic nanorings, Fano resonances, dense-array theory*

Multiresonant plasmonic nanoantennas offer possibilities for broadband sensor devices,[1−6] efficient solar cell upconverters,[7] coherent control,[8] enhanced nonlinear interactions,[9−12] and ultrabright multiband single-photon sources working at optical and telecom frequencies.[13] From an application perspective, it is of utmost importance (a) to scale the fabrication process from individual nanoantennas to large arrays,[14,15] (b) to design plasmonic nanoantennas exploiting multiresonant behavior that can be experimentally realized, and (c) to have a relatively simple theoretical framework at hand to describe the optical properties of arrays in terms of the properties of the individual nanoantennas. In this contribution, we show how all of the aforementioned requirements can be achieved.

We consider plasmonic nanoantennas that consist of multiple concentrically aligned gold nanorings of different sizes (Figure 1), further denoted as multirings. They are similar to previously discussed nanoantennas made from rings and discs.[10,16−25] These nanoantennas are known to sustain Fano resonances.[19,21] In general, Fano resonances are considered to originate from the coupling of a bright mode and a dark mode. In most cases, the bright (continuum) mode is an electric-dipole mode. The dark (discrete) mode is typically an electric-quadrupole or a magnetic-dipole mode (or another higher-order multipole mode).[26−34] These higher-order multipole modes couple only weakly to free-space radiation. This causes a narrower line width of the resonance, and losses are ultimately dominated by absorption rather than by radiation. The spectral interference of bright and dark modes causes an asymmetric line shape in the

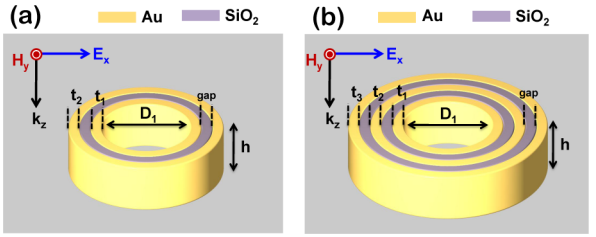

Figure 1. Schematic representation of nanoantennas in air made of multiple concentric plasmonic nanorings: (a) two gold nanorings; (b) three gold nanorings. The dielectric spacers have a refractive index of $n = 1.46$.

Received: March 19, 2015
Published: June 25, 2015

DOI: 10.1021/acsphotonics.5b00133
ACS Photonics 2015, 2, 1085−1090

scattering signal or in the reflectance and transmittance spectra of a periodic arrangement of the nanoantennas.

Nevertheless, different multipolar resonances are not required in order to observe Fano features.[26,27,35−37] What is usually considered as required is a largely disparate line width.[35] This line width can be tailored at the single-nanoantenna level. Indeed, it has been previously suggested that plasmonic ring structures experience lower absorption losses for thinner metallic rings or larger radii.[17−20] This renders their line width sufficiently narrow.

The lowest-order resonance of a plasmonic ring is electric-dipolar.[14,16,20,22] It is a bonding state of the hybridized surface plasmons at the inner and outer circumferences.[14,16,20,22] In the following we will demonstrate that higher-order modes in multirings are also solely dipolar. This offers the opportunity to have multiple narrow electric-dipolar resonances across a wide frequency range that spectrally interfere and cause a Fano line shape.

The emergence of spectrally overlapping resonances in the same scattering channel with equal angular momentum and polarization has only recently been suggested to lead to a scattering dark state.[38] For such a state, the scattering of a single nanoantenna is strongly suppressed. This phenomenon is robust against absorption, which makes the observation of scattering dark states with plasmonic structures feasible. We expect multirings to exhibit such states because they feature spectrally overlapping resonances. The appearance of scattering dark states can be understood not only in terms of a mutual coupling of the modes in the near field but also as a coherent interference in the far field.[38] For a periodic arrangement of such nanoantennas, the occurrence of scattering dark states shall translate into an asymmetric line-shape and a suppressed reflection at the frequency of the scattering dark state.

In this contribution, we theoretically and experimentally explore such phenomena with the example of a multiring nanoantenna. Contrary to the usual Fano schemes frequently discussed, the resonances of the multiring nanoantenna are entirely electric-dipolar in nature. This allows the use of a simple dense-array theory to predict the response of arrays of such nanoantennas from the scattering response of the individual constituents. With that, a very handy and versatile quasi-analytical theory is available that can predict the optical responses of macroscopic samples. This is similar to the description of Fano features in nanohole arrays.[36,37,39] Our theory provides unique insights into the design of metasurfaces whose optical properties can be understood not just by full-wave simulations but also by more analytically oriented theories.

NUMERICAL AND THEORETICAL RESULTS

Figure 1 shows a schematic of the studied multiring antenna. In all of the numerical simulations, the height of nanorings is h = 75 nm, and the diameter of the inner nanoring is D_1 = 100 nm. For now, the nanoantennas are embedded in vacuum and are illuminated by an x-polarized plane wave propagating in the z direction (Figure 1). The numerical calculations were performed with COMSOL.[40] The method solves Maxwell's equations in frequency space using a finite-element method. The dispersive permittivity of the gold was taken from ref 41. More details on the calculation of the total scattering cross section C_{sca} and p_x can be found in the literature.[42] In general, the numerically calculated scattered field is projected onto the analytically known fields of elementary multipolar sources. The multipole moments of the source are unambiguously retrieved by using a suitable normalization. Finally, the retrieved multipole moments are used to calculate their contributions to the total scattering cross section.[42,43]

Before considering a periodic array of multirings, we numerically investigate the scattering response of individual multirings. The total scattering cross sections as functions of frequency ν for multirings with two and three gold rings are shown in Figure 2a,b, respectively. The scattering responses of

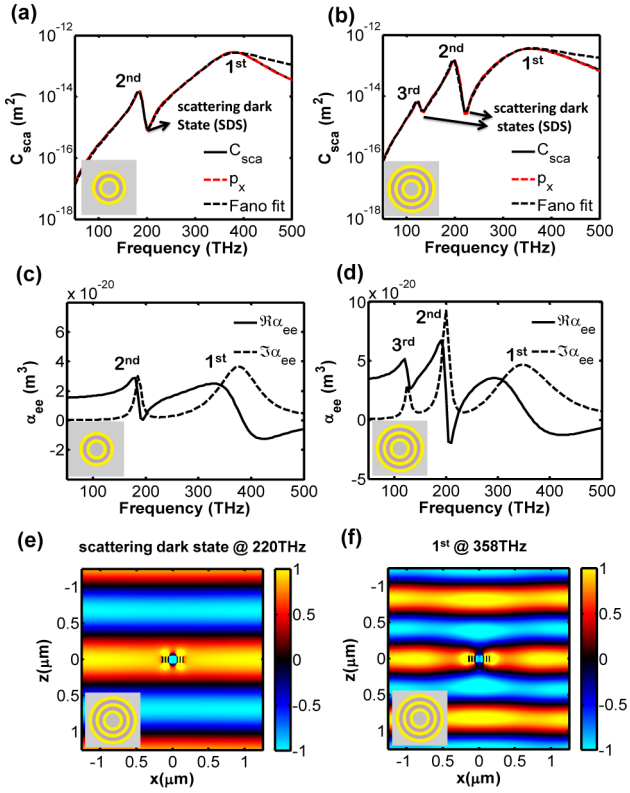

Figure 2. (a, b) Scattering cross sections (black lines) and the contributions to the scattering cross sections of the electric dipole moment (red dashed lines) as functions of frequency for (a) two and (b) three concentric nanorings. The black dashed lines show the Fano fits of the spectra. (c, d) The corresponding individual electric polarizabilities α_{ee} calculated by multipole expansion of the scattered field. (e, f) Field distributions (E_x) for (e) the scattering dark state (220 THz) and (f) the first mode (358 THz) of the three-ring configuration. The thickness of each layer (gold/dielectric) is $t_1 = t_2 = t_3$ = gap = 20 nm.

the nanoantennas are readily explained by their electric dipole moments (red dashed lines in Figure 2a,b); all of the higher-order multipoles are negligible.

For illumination with an x-polarized plane wave, the induced electric-dipole moment of the investigated nanoantennas can be calculated as $p_x = \varepsilon_0 \alpha_{ee} E_x$, since no cross-polarized electric dipole moments are induced. The real and imaginary parts of the electric polarizability α_{ee} are shown for the two- and three-ring systems in Figure 2c,d. The electric polarization indicates the existence of two or three modes for two or three gold rings, respectively. The line width of the first mode is very broad compared with those of the higher modes. Consequently, the first mode can be considered as a continuum mode, whereas the higher modes, which exhibit a larger quality factor, can be considered discrete. These higher-order modes are the dipolar

DOI: 10.1021/acsphotonics.5b00133
ACS Photonics 2015, 2, 1085−1090

Table 1. Parameters for the Fits to the Spectra Discussed in Figure 2a,b Using Equations 1 and 2 (Black Dashed Lines)[a]

	a^2 (m^2)	ν_s (THz)	W_s (THz)	ν_{a1} (THz)	ν_{a2} (THz)	W_{a1} (THz)	W_{a2} (THz)	q_1	q_2	b_1	b_2
Figure 2a	2.7×10^{-13}	365	60	185	–	8	–	−1.9	–	1	–
Figure 2b	2.95×10^{-13}	325	70	195	123	8	8	−3	−0.75	1	1.5

[a]It should be noted that Figure 2b has two Fano resonances (i.e. the second and third modes). ν_{a1} and ν_{a2} are the central frequencies of the second and third modes of the calculated spectra, respectively, and q_1 and q_2 are the corresponding asymmetric parameters.

resonances of rings with increasing radius. The resonance positions are clearly encountered as a resonant modulation in the total scattering cross section spectrum on top of the broad background caused by the first mode. Between the peaks, in the total scattering cross section spectrum, the scattering response is suppressed by coherent interference of the continuum and a discrete mode (Figure 2a,b). This phenomenon is known as a scattering dark state, which always appears between two scattering peaks[38] and can be due to a Fano resonance.[26] It is important to note again that the Fano resonance in the investigated multirings is due only to electric-dipole modes, which is different from the usually discussed plasmonic Fano resonances.[26] Scattering dark states exhibit a strongly suppressed scattering response in the far field (Figure 2a,b). For example, the three-ring nanoantenna is hardly visible at $\nu = 220$ THz (Figure 2e). At this frequency, the illumination causes a field enhancement in the near field, but the far field remains unperturbed. In contrast, the illumination is considerably scattered at the resonance frequency of the first mode (358 THz) (Figure 2f).

In order to quantitatively discuss the Fano features of the calculated spectra $C_{sca}(\nu)$ (see Figure 2a,b), we used a well-known fitting function. The fitting function is a product of the Fano line-shape function $C_{Fano}(\nu)$ and the Lorentzian line-shape function $C_{Lorentz}(\nu)$, i.e., $C_{sca}(\nu) = C_{Fano}(\nu)C_{Lorentz}(\nu)$.[33,44] The Fano line-shape function is given by

$$C_{Fano}(\nu) = \frac{\left(\frac{\nu^2 - \nu_a^2}{2W_a\nu_a} + q\right)^2 + b}{\left(\frac{\nu^2 - \nu_a^2}{2W_a\nu_a}\right)^2 + 1} \quad (1)$$

where q is the Fano (asymmetric) parameter, ν_a is the central frequency with spectral width W_a, and b is the modulation damping. Moreover, the Lorentzian line-shape reads as

$$C_{Lorentz}(\nu) = \left(\frac{\nu}{\nu_s}\right)^4 \frac{a^2}{\left(\frac{\nu^2 - \nu_s^2}{2W_s\nu_s}\right)^2 + 1} \quad (2)$$

where ν_s is the central frequency with spectral width W_s and a is the maximum amplitude of the resonance.[44] All of the fitting parameters for Figure 2a,b can be found in Table 1. It can be seen that the fitted spectra (the black dashed lines in Figure 2a,b) are in good agreement with the simulation results. The fitting parameters confirm a large asymmetry and thus Fano features in the simulated spectra.

In order to investigate the robustness of the observed optical features, i.e., the scattering dark state and the asymmetric Fano line shape, we calculated the scattering cross sections for two concentric nanorings with different dielectric spacers (i.e., gaps between the metallic rings). Figure 3a depicts the scattering cross sections for different dielectric spacers (i.e., gap = 20, 50, or 100 nm) as functions of frequency. It can be seen that the amplitude and bandwidth of the second mode can be widely tuned and enhanced by increasing the gap. However, the amplitude of the first mode is almost fixed. This allows to tune the position of the scattering dark state over a broad range of frequency (Figure 3b). Moreover, we calculated the scattering cross sections for various thicknesses of the outer gold ring. Examples are shown for t_2 = 20, 40, and 60 nm in Figure 4a. It can be seen that the amplitude and resonance position of the scattering dark state can be easily tuned by adopting this parameter as well (Figure 4b). Therefore, we can conclude that these features are quite robust against changes in the dimensions of the investigated nanoantenna.

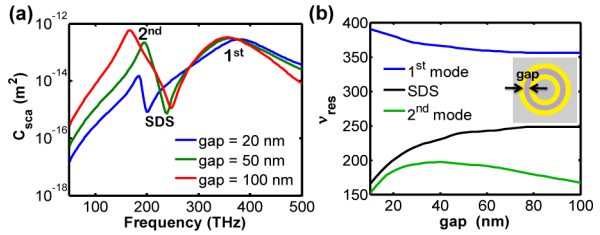

Figure 3. (a) Scattering cross sections for two concentric nanorings with different dielectric spacers (gaps) as functions of frequency. (b) Resonance frequencies of the first and second modes as well as the scattering dark state (SDS) as functions of the dielectric spacer (gap). The thickness of each gold layer is $t_1 = t_2 = 20$ nm.

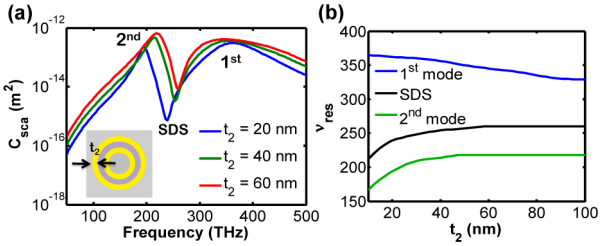

Figure 4. (a) Scattering cross sections for two concentric nanorings with different thicknesses of the outer gold ring (i.e., t_2 = 20, 40, or 60 nm) as functions of frequency. (b) Resonance frequency of the first and second modes as well as the scattering dark state (SDS) as functions of t_2. The thickness of first gold ring is $t_1 = 20$ nm, and the dielectric spacer is gap = 50 nm.

The scattering response of an isolated multiring at normal incidence can be solely explained by its electric polarizability α_{ee}. In the dipole approximation, a simplified dense-array theory can be used to calculate the reflection coefficient r and transmission coefficient t for a periodic array of these multirings:[42,45,46]

$$r = \frac{i\omega}{2\Lambda^2 c_0} \frac{\alpha_{ee}}{1 - \varepsilon_0 \alpha_{ee} \beta_{ee}} \quad (3)$$

$$t = 1 + \frac{i\omega}{2\Lambda^2 c_0} \frac{\alpha_{ee}}{1 - \varepsilon_0 \alpha_{ee} \beta_{ee}} \quad (4)$$

DOI: 10.1021/acsphotonics.5b00133
ACS Photonics 2015, 2, 1085−1090

where Λ is the period of the array, c_0 is the speed of light, ε_0 is the vacuum permittivity, and $\omega = 2\pi\nu$ is the angular frequency. The interaction constant β_{ee} is given by[45]

$$\beta_{ee} = i\frac{Z_0\omega}{4\Lambda^2}\left(1 + \frac{1}{ikR_0}\right)e^{ikR_0} \quad (5)$$

where $R_0 = \Lambda/1.438$ is the effective interparticle distance,[47] $Z_0 = 1/\varepsilon_0 c_0$ is the free-space impedance, and $k = \omega/c_0$ is the vacuum wavenumber. A monochromatic field ($\propto e^{-i\omega t}$) has been assumed. Reflection and transmission spectra based on eq 3 and eq 4, respectively, are sketched in Figure 5c,d and compared

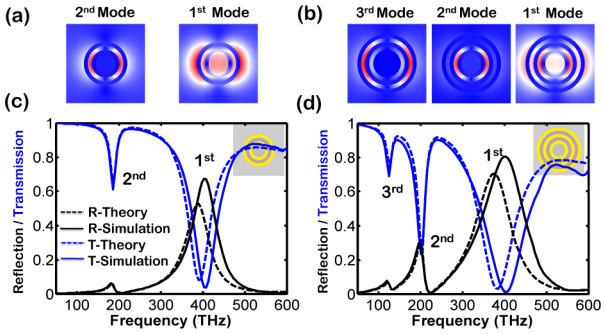

Figure 5. (a, b) Electric field distributions ($|\mathbf{E}|/|\mathbf{E}_{inc}|$) for all modes of the (a) two- and (b) three-concentric-nanoring structures, respectively. (c, d) Simulated (solid lines) and theoretical (dashed lines, based on eq 3 and eq 4) reflection (R) and transmission (T) spectra for arrays of (c) two- and (d) three-concentric-nanoring structures with period Λ = 500 nm. The thicknesses of the layers are $t_1 = t_2 = t_3$ = gap = 20 nm.

with the results of rigorous numerical simulations. At lower frequencies, the numerical results are in excellent agreement with the theory. A red shift of the numerical results occurs at higher frequencies because the wavelength becomes comparable to the actual size of the multirings and retardation effects come into play. As highlighted already, the strongly asymmetric line shapes of the reflection and transmission spectra are due to interference of different dipole modes. It is remarkable that over a small frequency range, e.g., between 200 and 220 THz for the three-gold-ring structure, the transmission and reflection of the array change drastically. Besides the Fano resonances, this is direct evidence of enhanced transmission of the scattering dark states as well. Whereas the scattering dark state is clearly visible in reflection, the transmission does not reach unity because of a remaining absorption (i.e., extinction remains finite).

The electric field distributions for all of the modes are shown in Figure 5a,b. The continuum (first) mode is dominated by the electric-dipolar response of the entire nanoantenna. This mode is super-radiant and leads to the large radiation-dominated line width. It provides a uniform field enhancement inside the innermost nanoring (Figure 5a). Similar modes can also be found in single-ring nanoantennas.[14−16,18,20] The higher-order modes are caused by antisymmetric coupling of dipolar modes of the individual rings, which effectively reduces their radiative yield. However, they do exhibit a net dipole moment in the far field. The higher-order modes are localized inside the dielectric spacer between two gold nanorings. Such highly concentrated gap modes might be used for coherent control,[8] to boost nonlinear effects,[9,10] or to access dipole-forbidden transitions of quantum systems.[48]

EXPERIMENTAL REALIZATION AND DISCUSSION

To underline the relevance and applicability of the investigated multirings, we extended our existing efficient and large-scale single-ring fabrication process to multirings. The basic process has been explained in detail in ref 15. Hence, we limit the following description to the basic fabrication scheme (Figure 6a). To fabricate the inner rings, resist pillars are generated on a

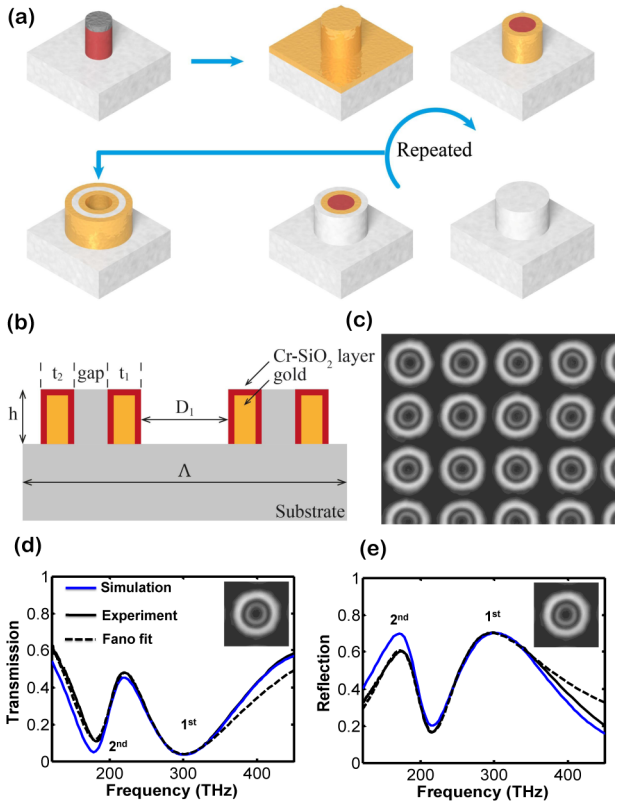

Figure 6. (a) Sketches of various steps in the fabrication of the investigated nanorings. (b) Sketch of the simulated structure. (c) Scanning electron microscopy image of the fabricated sample. (d, e) Simulated, measured, and corresponding Fano fits of the (d) transmission and (e) reflection spectra for two concentric gold nanorings. The dimensions of the two concentric nanorings were D_1 = 100 nm, t_1 = 23 nm, gap = 36 nm, and t_2 = 66 nm. The array was placed on a dielectric substrate (fused silica) with a refractive index of n = 1.46.

fused silica substrate by means of character projection electron beam lithography. In the next step, the resist pillars are homogeneously coated with gold by physical vapor deposition. To obtain a ring, the coating material is removed from horizontal surfaces by ion beam etching. The extension from a single ring to multirings was realized by repeating the coating and ion beam etching steps and alternating the coating material between gold and silicon dioxide. After assembly of the last concentric ring, the resist pillar in the core is removed by an oxygen plasma. Our approach allows the realization of multiring arrays with geometrical features and gaps below 20 nm and delivers a pattern efficiency of square decimeters in a reasonable time span of hours.[15,49] The measurements were performed using a PerkinElmer Lambda 950 spectrophotometer with unpolarized light.

We performed numerical simulations and compared them to the measured reflection and transmission of the fabricated

DOI: 10.1021/acsphotonics.5b00133
ACS Photonics 2015, 2, 1085−1090

samples. This provided evidence for the anticipated spectral features and allowed us to assess the quality of the samples (Figure 6d,e). Excellent agreement was observed upon consideration of fine details of the samples. Specifically, it was found that the involved etching processes cause redeposition of etched material at the metal interface of the nanorings. The redeposited material originates from the vicinity of the nanorings and is likely a mixture of silicon dioxide and chromium, which was used as the masking material for etching the resist pillars.

To precisely model the fabricated sample, those redepositions had to be considered in the simulations. Therefore, we used a very simplified model in complete analogy to that in ref 14. We introduced an additional homogeneous layer at the metal interfaces that were exposed to the ion beam during the etching process (Figure 6c). The optical properties of this layer are described by an effective index derived from an effective-medium theory considering a material consisting of 50% chromium and 50% silicon dioxide.[14] The geometrical parameters used in the simulation model were taken from scanning electron micrographs, i.e., D_1 = 100 nm, t_1 = 23 nm, gap = 36 nm, and t_2 = 66 nm. By fitting the simulation results to the measured spectra, we determined a thickness 3 nm for the layer describing the redeposited material. Despite the simplifications assumed in the model, it seems adequate to describe the experimental results.

In order to fit the measured reflection spectra to an analytical model and to extract the parameters that quantify the Fano features, we used an expression similar to that assumed for the scattering cross section based on eq 1 and eq 2:

$$R_{\mathrm{fit}} = \left[\frac{\left(\frac{\nu^2-\nu_a^2}{2W_a\nu_a}+q\right)^2+b}{\left(\frac{\nu^2-\nu_a^2}{2W_a\nu_a}\right)^2+1}\right]\left[\left(\frac{\nu}{\nu_s}\right)^2\frac{a^2}{\left(\frac{\nu^2-\nu_s^2}{2W_s\nu_s}\right)^2+1}\right] \quad (6)$$

It should be noted that the measured transmission spectrum is fitted by $1 - R_{\mathrm{fit}}$. All of the fitting parameters can be found in Table 2. The Fano parameters (i.e., q and b) confirm that the spectra possess notable asymmetric line shapes. However, enhanced transmission and scattering dark states are less pronounced. This is in fact related to the increased absorption of a 3 nm Cr−SiO_2 redeposited layer (see Figure 6b), which can be avoided, in general, by using another fabrication technique.[10] Moreover, the substrate also partially destroys these features. Nevertheless, they can be fully lifted by embedding the entire structure in a uniform medium with a refractive index corresponding to that of the substrate (SiO_2). Further simulations (not shown here) confirmed that these two features (scattering dark state and enhanced transmission) are pronounced for an ideal structure (i.e., without the Cr−SiO_2 redeposited layer) that is embedded in a homogeneous medium.

Table 2. Parameters for the Fits to the Spectra in Figure 6d,e Using Equation 6 (Black Dashed Lines)

	a^2	ν_s (THz)	W_s (THz)	ν_a (THz)	W_a (THz)	q	b
Figure 6d	1.05	210	136	196	38	−0.47	0.62
Figure 6e	0.98	216	110	194	38	−0.55	0.23

CONCLUSION

In conclusion, we have introduced a new type of multiresonant plasmonic nanoantenna based on concentric nanorings that shows some remarkable optical features, i.e., Fano resonances that cause enhanced and fully suppressed scattering. Dense-array theory can be applied to the investigated concentric nanorings to predict the optical response of an associated array based on the polarizability of the isolated nanoantennas. The numerically calculated response of such arrays agrees well with the dense-array predictions and experimental data. The distinguished field concentration of the modes inside the dielectric spacer makes concentric nanorings an interesting platform for enhanced light−matter interactions, especially for multiresonant systems. Furthermore, the fabrication method enables a large-scale, deterministic, and reproducible realization of multiresonant nanostructures with nanometric gaps.

AUTHOR INFORMATION

Corresponding Author

*E-mail: rasoul.khanghah@kit.edu.

Author Contributions

#R.A. and D.L. contributed equally.

Notes

The authors declare no competing financial interest.

ACKNOWLEDGMENTS

We thank the German Federal Ministry of Education and Research (PhoNa, 03IF2101A), the Thuringian State Government (MeMa, PE116-1), and the DFG Project MetaLiquid (KL 1199/6-1, RO 3640/3-1). The authors thank Dr. Ivan Fernandez-Corbaton for his constructive comments and suggestions.

REFERENCES

(1) Aydin, K.; Ferry, V. E.; Briggs, R. M.; Atwater, H. A. Broadband polarization-independent resonant light absorption using ultrathin plasmonic super absorbers. *Nat. Commun.* **2011**, *2*, 517.

(2) Alaee, R.; Menzel, C.; Huebner, U.; Pshenay-Severin, E.; bin Hasan, S.; Pertsch, T.; Rockstuhl, C.; Lederer, F. Deep-Subwavelength Plasmonic Nanoresonators Exploiting Extreme Coupling. *Nano Lett.* **2013**, *13*, 3482−3486.

(3) Huebner, U.; Pshenay-Severin, E.; Alaee, R.; Menzel, C.; Ziegler, M.; Rockstuhl, C.; Lederer, F.; Pertsch, T.; Meyer, H.-G.; Popp, J. Exploiting extreme coupling to realize a metamaterial perfect absorber. *Microelectron. Eng.* **2013**, *111*, 110−113.

(4) Liu, N.; Mesch, M.; Weiss, T.; Hentschel, M.; Giessen, H. Infrared Perfect Absorber and Its Application As Plasmonic Sensor. *Nano Lett.* **2010**, *10*, 2342−2348.

(5) Monticone, F.; Argyropoulos, C.; Alù, A. Multilayered Plasmonic Covers for Comblike Scattering Response and Optical Tagging. *Phys. Rev. Lett.* **2013**, *110*, 113901.

(6) Monticone, F.; Argyropoulos, C.; Alu, A. Layered plasmonic cloaks to tailor the optical scattering at the nanoscale. *Sci. Rep.* **2012**, *2*, 912 DOI: 10.1038/srep00912.

(7) Atwater, H. A.; Polman, A. Plasmonics for improved photovoltaic devices. *Nat. Mater.* **2010**, *9*, 205−213.

(8) Leveque, G.; Martin, O. Narrow-band multiresonant plasmon nanostructure for the coherent control of light: an optical analog of the xylophone. *Phys. Rev. Lett.* **2008**, *100*, 117402.

(9) Metzger, B.; Schumacher, T.; Hentschel, M.; Lippitz, M.; Giessen, H. Third Harmonic Mechanism in Complex Plasmonic Fano Structures. *ACS Photonics* **2014**, *1*, 471−476.

(10) Lehr, D.; Reinhold, J.; Thiele, I.; Hartung, H.; Dietrich, K.; Menzel, C.; Pertsch, T.; Kley, E.-B.; Tünnermann, A. Enhancing

DOI: 10.1021/acsphotonics.5b00133
ACS Photonics 2015, 2, 1085−1090

Second Harmonic Generation in Gold Nanoring Resonators Filled with Lithium Niobate. *Nano Lett.* **2015**, *15*, 1025−1030.
(11) Linden, S.; Niesler, F. B. P.; Förstner, J.; Grynko, Y.; Meier, T.; Wegener, M. Collective Effects in Second-Harmonic Generation from Split-Ring-Resonator Arrays. *Phys. Rev. Lett.* **2012**, *109*, 015502.
(12) Cai, W.; Vasudev, A. P.; Brongersma, M. L. Electrically Controlled Nonlinear Generation of Light with Plasmonics. *Science* **2011**, *333*, 1720−1723.
(13) Filter, R.; Słowik, K.; Straubel, J.; Lederer, F.; Rockstuhl, C. Nanoantennas for ultrabright single photon sources. *Opt. Lett.* **2014**, *39*, 1246−1249.
(14) Lehr, D.; Dietrich, K.; Helgert, C.; Käsebier, T.; Fuchs, H.-J.; Tünnermann, A.; Kley, E.-B. Plasmonic properties of aluminum nanorings generated by double patterning. *Opt. Lett.* **2012**, *37*, 157−159.
(15) Lehr, D.; Alaee, R.; Filter, R.; Dietrich, K.; Siefke, T.; Rockstuhl, C.; Lederer, F.; Kley, E.-B.; Tünnermann, A. Plasmonic nanoring fabrication tuned to pitch: Efficient, deterministic, and large scale realization of ultra-small gaps for next generation plasmonic devices. *Appl. Phys. Lett.* **2014**, *105*, 143110.
(16) Aizpurua, J.; Hanarp, P.; Sutherland, D. S.; Käll, M.; Bryant, G. W.; Garcia de Abajo, F. J. Optical Properties of Gold Nanorings. *Phys. Rev. Lett.* **2003**, *90*, 057401.
(17) Hao, F.; Nordlander, P.; Burnett, M. T.; Maier, S. A. Enhanced tunability and linewidth sharpening of plasmon resonances in hybridized metallic ring/disk nanocavities. *Phys. Rev. B* **2007**, *76*, 245417.
(18) Hao, F.; Larsson, E. M.; Ali, T. A.; Sutherland, D. S.; Nordlander, P. Shedding light on dark plasmons in gold nanorings. *Chem. Phys. Lett.* **2008**, *458*, 262−266.
(19) Hao, F.; Nordlander, P.; Sonnefraud, Y.; Dorpe, P. V.; Maier, S. A. Tunability of Subradiant Dipolar and Fano-Type Plasmon Resonances in Metallic Ring/Disk Cavities: Implications for Nanoscale Optical Sensing. *ACS Nano* **2009**, *3*, 643−652.
(20) Nordlander, P. The Ring: A Leitmotif in Plasmonics. *ACS Nano* **2009**, *3*, 488−492.
(21) Sonnefraud, Y.; Verellen, N.; Sobhani, H.; Vandenbosch, G. A.; Moshchalkov, V. V.; van Dorpe, P.; Nordlander, P.; Maier, S. A. Experimental Realization of Subradiant, Superradiant, and Fano Resonances in Ring/Disk Plasmonic Nanocavities. *ACS Nano* **2010**, *4*, 1664−1670.
(22) Tsai, C.-Y.; Lu, S.-P.; Lin, J.-W.; Lee, P.-T. High sensitivity plasmonic index sensor using slablike gold nanoring arrays. *Appl. Phys. Lett.* **2011**, *98*, 153108.
(23) Near, R.; Tabor, C.; Duan, J.; Pachter, R.; El-Sayed, M. Pronounced Effects of Anisotropy on Plasmonic Properties of Nanorings Fabricated by Electron Beam Lithography. *Nano Lett.* **2012**, *12*, 2158−2164.
(24) Toma, M.; Cho, K.; Wood, J.; Corn, R. Gold Nanoring Arrays for Near Infrared Plasmonic Biosensing. *Plasmonics* **2014**, *9*, 765−772.
(25) Rakovich, A.; Albella, P.; Maier, S. A. Plasmonic Control of Radiative Properties of Semiconductor Quantum Dots Coupled to Plasmonic Ring Cavities. *ACS Nano* **2015**, *9*, 2648−2658.
(26) Miroshnichenko, A. E.; Flach, S.; Kivshar, Y. S. Fano resonances in nanoscale structures. *Rev. Mod. Phys.* **2010**, *82*, 2257−2298.
(27) Luk'yanchuk, B.; Zheludev, N. I.; Maier, S. A.; Halas, N. J.; Nordlander, P.; Giessen, H.; Chong, C. T. The Fano resonance in plasmonic nanostructures and metamaterials. *Nat. Mater.* **2010**, *9*, 707−715.
(28) Liu, W.; Miroshnichenko, A. E.; Kivshar, Y. S. Control of light scattering by nanoparticles with optically-induced magnetic responses. *Chin. Phys. B* **2014**, *23*, 047806.
(29) Singh, R.; Al-Naib, I. A. I.; Koch, M.; Zhang, W. Sharp Fano resonances in THz metamaterials. *Opt. Express* **2011**, *19*, 6312−6319.
(30) Zhao, J.; Zhang, C.; Braun, P. V.; Giessen, H. Large-Area Low-Cost Plasmonic Nanostructures in the NIR for Fano Resonant Sensing. *Adv. Mater.* **2012**, *24*, OP247−OP252.
(31) Liu, W.; Miroshnichenko, A. E.; Neshev, D. N.; Kivshar, Y. S. Polarization-independent Fano resonances in arrays of core-shell nanoparticles. *Phys. Rev. B* **2012**, *86*, 081407.
(32) Ruan, Z.; Fan, S. Superscattering of Light from Subwavelength Nanostructures. *Phys. Rev. Lett.* **2010**, *105*, 013901.
(33) Gallinet, B.; Martin, O. J. F. Ab initio theory of Fano resonances in plasmonic nanostructures and metamaterials. *Phys. Rev. B* **2011**, *83*, 235427.
(34) Hancu, I. M.; Curto, A. G.; Castro-López, M.; Kuttge, M.; van Hulst, N. F. Multipolar interference for directed light emission. *Nano Lett.* **2014**, *14*, 166−171.
(35) Fano, U. Effects of Configuration Interaction on Intensities and Phase Shifts. *Phys. Rev.* **1961**, *124*, 1866−1878.
(36) Genet, C.; van Exter, M.; Woerdman, J. Fano-type interpretation of red shifts and red tails in hole array transmission spectra. *Opt. Commun.* **2003**, *225*, 331−336.
(37) Sarrazin, M.; Vigneron, J.-P.; Vigoureux, J.-M. Role of Wood anomalies in optical properties of thin metallic films with a bidimensional array of subwavelength holes. *Phys. Rev. B* **2003**, *67*, 085415.
(38) Hsu, C. W.; DeLacy, B. G.; Johnson, S. G.; Joannopoulos, J. D.; Soljacic, M. Theoretical Criteria for Scattering Dark States in Nanostructured Particles. *Nano Lett.* **2014**, *14*, 2783−2788.
(39) Altewischer, E.; Ma, X.; van Exter, M. P.; Woerdman, J. P. Fano-type interference in the point-spread function of nanohole arrays. *Opt. Lett.* **2005**, *30*, 2436−2438.
(40) *COMSOL Multiphysics User's Guide*, version 4.3; COMSOL: Burlington, MA, 2012.
(41) Johnson, P. B.; Christy, R. W. Optical Constants of the Noble Metals. *Phys. Rev. B* **1972**, *6*, 4370−4379.
(42) Mühlig, S.; Menzel, C.; Rockstuhl, C.; Lederer, F. Multipole analysis of meta-atoms. *Metamaterials* **2011**, *5*, 64−73.
(43) Bernal Arango, F.; Coenen, T.; Koenderink, A. F. Underpinning Hybridization Intuition for Complex Nanoantennas by Magneto-electric Quadrupolar Polarizability Retrieval. *ACS Photonics* **2014**, *1*, 444−453.
(44) Gallinet, B.; Martin, O. J. F. Influence of Electromagnetic Interactions on the Line Shape of Plasmonic Fano Resonances. *ACS Nano* **2011**, *5*, 8999−9008.
(45) Tretyakov, S. *Analytical Modeling in Applied Electromagnetics*; Artech House: Norwood, MA, 2003.
(46) Alaee, R.; Albooyeh, M.; Yazdi, M.; Komjani, N.; Simovski, C.; Lederer, F.; Rockstuhl, C. Magnetoelectric coupling in nonidentical plasmonic nanoparticles: Theory and applications. *Phys. Rev. B* **2015**, *91*, 115119.
(47) Collin, R. E. *Field Theory of Guided Waves*; McGraw-Hill: New York, 1960.
(48) Filter, R.; Mühlig, S.; Eichelkraut, T.; Rockstuhl, C.; Lederer, F. Controlling the dynamics of quantum mechanical systems sustaining dipole-forbidden transitions via optical nanoantennas. *Phys. Rev. B* **2012**, *86*, 035404.
(49) Kley, E.-B.; Schmidt, H.; Zeitner, U.; Banasch, M.; Schnabel, B. Enhanced e-beam pattern writing for nano-optics based on character projection. 28th European Mask and Lithography Conference (EMLC 2012), 2012, 83520M; DOI: 10.1117/12.920562.

DOI: 10.1021/acsphotonics.5b00133
ACS Photonics 2015, 2, 1085−1090